QUARTERLY JOURNAL OF THE ROYAL METEOROLOGICAL SOCIETY
Q. J. R. Meteorol. Soc. **135**: 839–850 (2009)
Published online 15 April 2009 in Wiley InterScience
(www.interscience.wiley.com) DOI: 10.1002/qj.390

Limitations of a linear model for the hurricane boundary layer

Stefanie Vogl and Roger K. Smith*
Meteorological Institute, University of Munich, Germany

ABSTRACT: The linear model for the steady boundary layer of a rapidly rotating axisymmetric vortex is derived from a detailed scale analysis of the full equations of motion. The previously known analytic solution is re-appraised for vortices of hurricane scale and strength. The internal consistency of the linear approximation is investigated for such a vortex by calculating from the solution the magnitude of the nonlinear terms that are neglected in the approximation compared with the terms retained. It is shown that the nonlinear terms are not negligibly small in a large region of the vortex, a feature that is consistent with the scale analysis. We argue that the boundary-layer problem is well-posed only at outer radii where there is subsidence into the layer. At inner radii, where there is ascent, only the radial pressure gradient may be prescribed and not the wind components at the top of the boundary layer, but the linear problem cannot be solved in these circumstances. We examine the radius at which the vertical flow at the top of the boundary layer changes sign for different tangential wind profiles relevant to hurricanes and show that this is several hundred kilometres from the vortex centre. This feature represents a further limitation of the linear model applied to hurricanes. While the present analysis assumes axial symmetry, the same limitations presumably apply to non-axisymmetric extensions to the linear model. Copyright © 2009 Royal Meteorological Society

KEY WORDS hurricanes; tropical cyclones; typhoons; boundary layer; friction layer

Received 21 October 2008; Revised 14 January 2009; Accepted 22 January 2009

1. Introduction

The boundary layer of a mature hurricane is an important feature of the storm, as it strongly constrains the radial distribution of vertical motion at its top, as well as the distributions of absolute angular momentum and moisture. In fact, there is mounting evidence that the boundary layer plays a central role in the hurricane intensification process itself (e.g. Emanuel, 1997; Smith *et al.*, 2008, 2009). Over the years the boundary layer has been the subject of numerous theoretical investigations, many of them relating to axisymmetric vortices (Rosenthal, 1962; Miller, 1965; Smith, 1968; Leslie and Smith, 1970; Carrier, 1971; Eliassen, 1971; Bode and Smith, 1975; Eliassen and Lystadt, 1977; Montgomery *et al.*, 2001; Smith, 2003; Smith and Montgomery, 2008; Smith and Vogl, 2008) and a few also to asymmetric vortices (Shapiro, 1983; Kepert, 2001; Kepert and Wang, 2001). These studies can be divided into three types: vertically integrated models that assume certain profiles of the radial and tangential wind components, but not their scales (Smith, 1968; Leslie and Smith, 1970; Bode and Smith, 1975); slab models, which are a subset of the former that assume uniform profiles (Shapiro, 1983; Smith, 2003; Smith and Vogl, 2008; Smith and Montgomery, 2008); and what we will term 'continuous models', in which the vertical structure is determined as well as the radial structure (Eliassen, 1971; Eliassen and Lystadt, 1977; Montgomery *et al.*, 2001; Kepert, 2001; Kepert and Wang, 2001). With the exception of Smith (2003) and Smith and Vogl (2008), all of the aforementioned studies have focused on the dynamical aspects of the boundary layer: thermodynamic aspects were not considered.

In one of the early studies, Eliassen (1971) developed a linear theory for the spin-down of a vortex as a result of surface friction and showed that, if a no-slip condition is applied at the surface, the temporal decay of the tangential winds above the boundary layer is exponential. He showed also that the vertical velocity at the top of the boundary layer is upwards and nearly constant inside the radius of maximum tangential winds, with a maximum at the vortex centre. However, in the case of a turbulent boundary layer, the vortex decays algebraically with time. Moreover, the vertical velocity at the top of the boundary layer is zero at the vortex centre and increases linearly with radius inside the radius of maximum tangential winds.

Eliassen and Lystadt (1977) extended this work to account for differential rotation in the tangential flow and presented numerical solutions of the coupled equations for the boundary layer and the vortex above for the case with a quadratic drag law in the surface layer. Their spin-down theory predicts the evolution of the angular velocity, the transverse streamfunction and the boundary-layer depth, as well as the half-life time of the vortex (the time

*Correspondence to: Roger K. Smith, Meteorological Institute, University of Munich, Theresienstr. 37, 80333 Munich, Germany.
E-mail: roger.smith@lmu.de

required to reduce the angular velocity by one half). The theory is formulated in an inertial (non-rotating) coordinate system and assumes that the flow evolves close to a state of cyclostrophic balance throughout the fluid. However, the strongest vortex examined had a maximum speed of only 10 m s^{-1}, corresponding to a Rossby number of 20 at the latitude considered. Montgomery *et al.* (2001) pointed out that the neglected non-cyclostrophic terms in the boundary layer may become significant at higher swirl speeds, which might limit the applicability of the theory to hurricanes. To investigate this issue they performed numerical calculations of the full nonlinear equations in the same spin-down flow configuration as Eliassen and Lystadt, and obtained solutions for vortices of different intensities including hurricane-strength vortices (i.e. with maximum tangential winds exceeding 33 m s^{-1}). They found that the theoretically predicted algebraic temporal decay of the primary vortex is validated also for tropical storm and hurricane-strength vortices, but noted increasing quantitative departures from Eliassen and Lystadt's theory with increasing fluid depth, although it is still qualitatively valid for hurricane-like vortices 10 and 15 km deep. They found also that, as the vortex strength increases from tropical storm to hurricane strength, the cyclostrophic balance approximation becomes only marginally valid in the boundary layer yet remains valid in the flow interior. In addition, a temporary spin-up of tangential winds and vertical vorticity in the boundary layer and a low-level outflow jet occurred in the numerical simulations, features that are not predicted by the theory. These features were argued to be the primary cause for the discrepancy between the theory and the model simulations.

Kepert (2001) examined the linear equations for the steady boundary layer of an asymmetric vortex and obtained an analytic solution to these. The theory reduces to that derived by Eliassen and Lystadt (1977) in the axisymmetric case. The solution was shown to exhibit a region of supergradient winds near the top of the layer just like the Ekman solution and, as in the Ekman solution, the degree to which the flow is supergradient was only a few percent. In a companion paper, Kepert and Wang (2001) compared their linear solution with a steady-state solution for the boundary layer obtained from a numerical model, which included a relatively sophisticated parameterization of the boundary layer. They showed, inter alia, that vertical advection of angular momentum plays a crucial role in strengthening the supergradient component, which may be several times stronger than predicted by the linear model.

Recently, Smith and Montgomery (2008) examined various approximations to the full nonlinear equations for a slab boundary layer in the axisymmetric case and showed that the linear theory was rather poor in capturing the radial structure of the boundary layer when compared with numerical solutions of the corresponding nonlinear equations. In the slab case, the boundary layer in the linear approximation cannot be supergradient. These authors showed that the assumption of gradient wind balance in the boundary layer was poor also. In particular, the radius at which the vertical flow at the top of the boundary layer changes sign from subsidence at outer radii to upflow at inner radii is much larger in the linear and balanced solutions than in the nonlinear control solution. The poorness of the linear and balanced solutions is consistent with a detailed scale analysis for a slab boundary-layer model.

The slab model has one particular deficiency in that it does not provide a means to determine the radial variation of the boundary-layer depth, and it is necessary to appeal to the scaling analysis of the continuous model to incorporate this variation in the model. However it does have the advantage that it is not necessary that the flow leaving the boundary layer be constrained to be in gradient wind balance with that above the boundary layer (Smith and Vogl, 2008). Neither Eliassen and Lystadt (1977) nor Kepert (2001) carried out a detailed scale analysis to underpin the linear approximation and the results of Montgomery *et al.* (2001) and Smith and Montgomery (2008) cast serious doubts on its accuracy when applied to hurricanes, especially in the inner core region. Even so, it remains of intrinsic scientific interest because it is an extension of the classical Ekman boundary-layer theory and because it may be solved analytically.

In this article we show how the linear approximation may be derived from a detailed scale analysis of the Navier–Stokes equations, assuming that turbulent stresses can be represented by an eddy diffusivity formulation. We examine also the self-consistency of the approximation by computing the nonlinear terms that are neglected in the derivation of the theory from solutions obtained from the theory. Finally we examine the extent to which the accuracy of the linear approximation depends on the profile of the imposed tangential wind field at the top of the boundary layer.

The paper is organized as follows. In section 2 we review the full set of equations and carry out a detailed scale analysis of them. On the basis of this analysis we derive the full u- and v-momentum equations in the boundary layer and the linear approximation thereto. We give also the analytic solution to the linear problem. In section 3 we show plots of solutions of the linear equations and examine the consistency of the approximation by comparing the magnitude of the neglected nonlinear terms with that of the linear terms retained. Section 4 discusses a range of issues concerning the linear theory and our conclusions are presented in section 5.

2. Boundary-layer equations

The boundary layer of a hurricane is relatively shallow, typically less than 1 km deep, so that the variation of density with height can be neglected to a good approximation. Assuming for the present that the turbulent momentum transfer may be represented in terms of a constant eddy diffusivity, K, the Navier–Stokes equations for an axisymmetric vortex may be expressed in

DOI: 10.1002/qj

cylindrical polar coordinates (r, λ, z) as

$$\frac{\partial u}{\partial t} + u\frac{\partial u}{\partial r} + w\frac{\partial u}{\partial z} - \frac{v^2}{r} - fv = -\frac{1}{\rho}\frac{\partial p}{\partial r} + K\left(\nabla^2 u - \frac{u}{r^2}\right), \quad (1)$$

$$\frac{\partial v}{\partial t} + u\frac{\partial v}{\partial r} + w\frac{\partial v}{\partial z} + \frac{uv}{r} + fu = K\left(\nabla^2 v - \frac{v}{r^2}\right), \quad (2)$$

$$\frac{\partial w}{\partial t} + u\frac{\partial w}{\partial r} + w\frac{\partial w}{\partial z} = -\frac{1}{\rho}\frac{\partial p}{\partial z} + K\nabla^2 w, \quad (3)$$

where (u, v, w) is the velocity vector, p is the perturbation pressure, and ρ is the density. The equations are supplemented by the continuity equation, which for a homogeneous fluid is

$$\frac{1}{r}\frac{\partial ru}{\partial r} + \frac{\partial w}{\partial z} = 0. \quad (4)$$

In the derivation of equations for the boundary layer it is normally assumed that the tangential wind component, v_g, at the top of the boundary layer is a function only of radius and possibly time and that it is in gradient wind balance, i.e. it satisfies the equation

$$\frac{v_g^2}{r} + fv_g = \frac{1}{\rho}\frac{\partial p}{\partial r}. \quad (5)$$

We will show below that the radial pressure gradient throughout the boundary layer is, to a close approximation, equal to that at the top of the layer. This result allows us to substitute for the pressure gradient in terms of v_g using (5). Then, setting $v = v_g(r, t) + v'$, Equations (1) and (2) become

$$\frac{\partial u}{\partial t} + u\frac{\partial u}{\partial r} + w\frac{\partial u}{\partial z} - \frac{v'^2}{r} - \xi_g v' = K\left(\nabla^2 u - \frac{u}{r^2}\right), \quad (6)$$

$$\frac{\partial v'}{\partial t} + u\frac{\partial v'}{\partial r} + w\frac{\partial v'}{\partial z} + \frac{uv'}{r} + \zeta_{ag} u = K\left(\nabla^2 v - \frac{v}{r^2}\right), \quad (7)$$

where

$$\xi_g = \frac{2v_g}{r} + f \qquad \text{and} \qquad \zeta_{ag} = \frac{\mathrm{d}v_g}{\mathrm{d}r} + \frac{v_g}{r} + f \quad (8)$$

are the absolute angular velocity and vertical component of absolute vorticity of the gradient wind, respectively.

It is instructive at the outset to carry out a detailed scale analysis of these equations.

2.1. Scale analysis

Let U, V, V', W be scales for u, v, v', w, and R, Z be length-scales for r and z, respectively. Let $T = R/U$ be an advective time-scale for the radial flow and Δp a scale for changes in the perturbation pressure, p.

We examine first the continuity equation (Equation (4)). The two terms of on the left-hand side have scales

$$\frac{U}{R}, \qquad \frac{W}{Z},$$

and since these sum to zero they must have the same magnitude, i.e. $W/Z \sim U/R$. This result is used to simplify the scale analysis of the momentum equations shown in Tables I and II. The ratios in the first lines under each equation in these tables show the scale of the equation term above it, while the second lines show the corresponding non-dimensional scale. The latter scales are obtained by dividing line (3a) in Table I by V^2/Z to obtain (3b), dividing line (6a) in Table II by $V'\Xi$ to obtain (6b), and dividing line (7a) in Table II by $U\Lambda$ to obtain (7b). Here Ξ is taken as a scale for ξ_g and Λ as a scale for for ζ_{ag}. It is seen that the analysis introduces six nondimensional parameters:

- $Ro_\Lambda = V/(R\Lambda)$, a local Rossby number in the tangential momentum equation based on the gradient wind (scale V) and the local absolute vorticity of the gradient wind above the boundary layer (Λ);
- $Ro_\Xi = V/(R\Xi)$, a local Rossby number in the radial momentum equation based on twice the absolute rotation rate of the gradient wind, Ξ, instead of Λ;
- $S_u = U/V$, the ratio of the radial to tangential wind speed;
- $S_{v'} = V'/V$, the ratio of the departure of the tangential wind speed from the gradient wind to the gradient wind itself;
- $R_e = VZ/K$, a *Reynolds number*, which characterizes the importance of the inertial to the friction terms;
- $A = Z/R$, an aspect ratio, which measures the ratio of the boundary-layer depth to the radial scale.

As we assume the motion to be axisymmetric, a separate advective time-scale for the tangential flow, V/R, is not required.

We consider first the vertical momentum equation. Typically, the boundary layer is thin, somewhere between 500 m to 1 km in depth, whereupon the aspect ratio $A = Z/R$ is small compared with unity. Moreover, typical values of K are on the order of 10 m s^{-2}, at least outside the strong wind region of the vortex core. Taking $V = 50$ m s^{-1} and $R = 50$ km, characteristic of the inner core region, and $Z = 500$ m gives $R_e = 2.5 \times 10^3$ and $A = 10^{-2}$. It follows from line (7b) in Table I that $\Delta p/(\rho V^2) \approx \max(S_u^2 A^2,\ S_u A R_e^{-1}) = 1.0 \times 10^{-4}$, even assuming that $S_u \approx 1$ in the boundary layer. Thus the vertical variation of p across the boundary layer is only a tiny fraction of the radial variation of p above the

DOI: 10.1002/qj

Table I. Scaling of the terms in Equation (3). Here $\nabla_h^2 = (\partial/\partial r)(r\partial/\partial r)$, $A = Z/R$, $S_u = U/V$ and $R_e = VZ/K$.

			w-momentum			
$\frac{\partial w}{\partial t}$	$+u\frac{\partial w}{\partial r}$	$+w\frac{\partial w}{\partial z}$	$= -\frac{1}{\rho}\frac{\partial p}{\partial z}$	$+K\nabla_h^2 w$	$+K\frac{\partial^2 w}{\partial z^2}$	(3)
$\frac{W}{T}$	$\frac{UW}{R}$	$\frac{WW}{Z}$	$\frac{\Delta p}{\rho Z}$	$K\frac{W}{R^2}$	$K\frac{W}{Z^2}$	(3a)
$S_u^2 A^2$	$S_u^2 A^2$	$S_u^2 A^2$	$\frac{\Delta p}{\rho V^2}$	$S_u A^3 R_e^{-1}$	$S_u A R_e^{-1}$	(3b)

Table II. Scaling of the terms in Equations (6) and (7). Here $\nabla_h^2 = (\partial/\partial r)(r\partial/\partial r)$, $A = Z/R$, $S_u = U/V$, $S_{v'} = V'/V$, $Ro_\Xi = V/(R\Xi)$, $Ro_\Lambda = V/(R\Lambda)$ and $R_e = VZ/K$. Note that v is not replaced by v' in the penultimate term in (7b) because v_g depends on r.

				u-momentum			
$\frac{\partial u}{\partial t}$	$+u\frac{\partial u}{\partial r}$	$+w\frac{\partial u}{\partial z}$	$-\frac{v'^2}{r}$	$-\xi_g v' =$	$+K\left(\nabla_h^2 u - \frac{u}{r^2}\right)$	$+K\frac{\partial^2 u}{\partial z^2}$	(6)
$\frac{U}{T}$	$\frac{U^2}{R}$	$W\frac{U}{Z}$	$\frac{V'^2}{R}$	$\Xi V'$	$K\frac{U}{R^2}$	$K\frac{U}{Z^2}$	(6a)
$S_u^2 S_{v'}^{-1} Ro_\Xi$	$S_u^2 S_{v'}^{-1} Ro_\Xi$	$S_u^2 S_{v'}^{-1} Ro_\Xi$	$S_{v'} Ro_\Xi$	1	$A(R_e S_{v'})^{-1} S_u Ro_\Xi$	$(AR_e S_{v'})^{-1} S_u Ro_\Xi$	(6b)
				v-momentum			
$\frac{\partial v'}{\partial t}$	$+u\frac{\partial v'}{\partial r}$	$+w\frac{\partial v'}{\partial z}$	$+\frac{uv'}{r}$	$+\zeta_{ag} u =$	$+K\left(\nabla_h^2 v - \frac{v}{r^2}\right)$	$+K\frac{\partial^2 v'}{\partial z^2}$	(7)
$\frac{V'}{T}$	$U\frac{V'}{R}$	$W\frac{V'}{Z}$	$U\frac{V'}{R}$	ΛU	$K\frac{V}{R^2}$	$K\frac{V'}{Z^2}$	(7a)
$S_{v'} Ro_\Lambda$	$S_{v'} Ro_\Lambda$	$S_{v'} Ro_\Lambda$	$S_{v'} Ro_\Lambda$	1	$A(R_e S_u)^{-1} Ro_\Lambda$	$(AR_e S_u)^{-1} S_{v'} Ro_\Lambda$	(7b)

boundary layer. In other words, to a close approximation, *the radial pressure gradient within the boundary layer is the same as that at the top of the boundary layer*. This result enables the pressure gradient in the boundary layer to be replaced by the gradient wind at the top of the layer, as was done in deriving Equations (6) and (7).

We examine now the terms in the radial and tangential components of the momentum equation. First we note that the radial diffusion term is $O(A^2)$ times that of the vertical diffusion term in (6a) and $O(A^2 S_{v'}^{-1})$ that of the vertical diffusion term in (7a). Thus even if $S_{v'}$ is as small as $O(10^{-3})$, both terms representing radial diffusion can be neglected.

From Table II, we see that a vertical scale Z that makes the largest friction terms as important as the linear terms in (6a) and (7a) is such that $\Xi V' \approx KU/Z^2$ and $\Lambda U \approx KV'/Z^2$, from which it follows that $Z = (K/I^*)^{1/2}$, where $I^{*2} = \Lambda\Xi$ is a scale for the inertial stability parameter defined by $I^2 = \xi_g \zeta_{ag}$. If $Ro = V/(Rf) \ll 1$, ξ_g and ζ_{ag} are both approximately equal to f and the vertical scale reduces to $(K/f)^{1/2}$, which is the appropriate scaling for the classical Ekman layer.

2.2. The full boundary-layer equations

From the scale analysis in Tables I and II, the full radial and tangential momentum equations in the boundary layer are

$$\frac{\partial u}{\partial t} + u\frac{\partial u}{\partial r} + w\frac{\partial u}{\partial z} - \frac{v'^2}{r} - \xi_g v' = K\frac{\partial^2 u}{\partial z^2} \qquad (9)$$

and

$$\frac{\partial v'}{\partial t} + u\frac{\partial v'}{\partial r} + w\frac{\partial v'}{\partial z} + \frac{uv'}{r} + \zeta_{ag} u = K\frac{\partial^2 v'}{\partial z^2}. \qquad (10)$$

These are supplemented by the continuity equation (4).

Further approximations are not possible without knowledge of the radial variation of Ro_Ξ and Ro_Λ as well as

DOI: 10.1002/qj

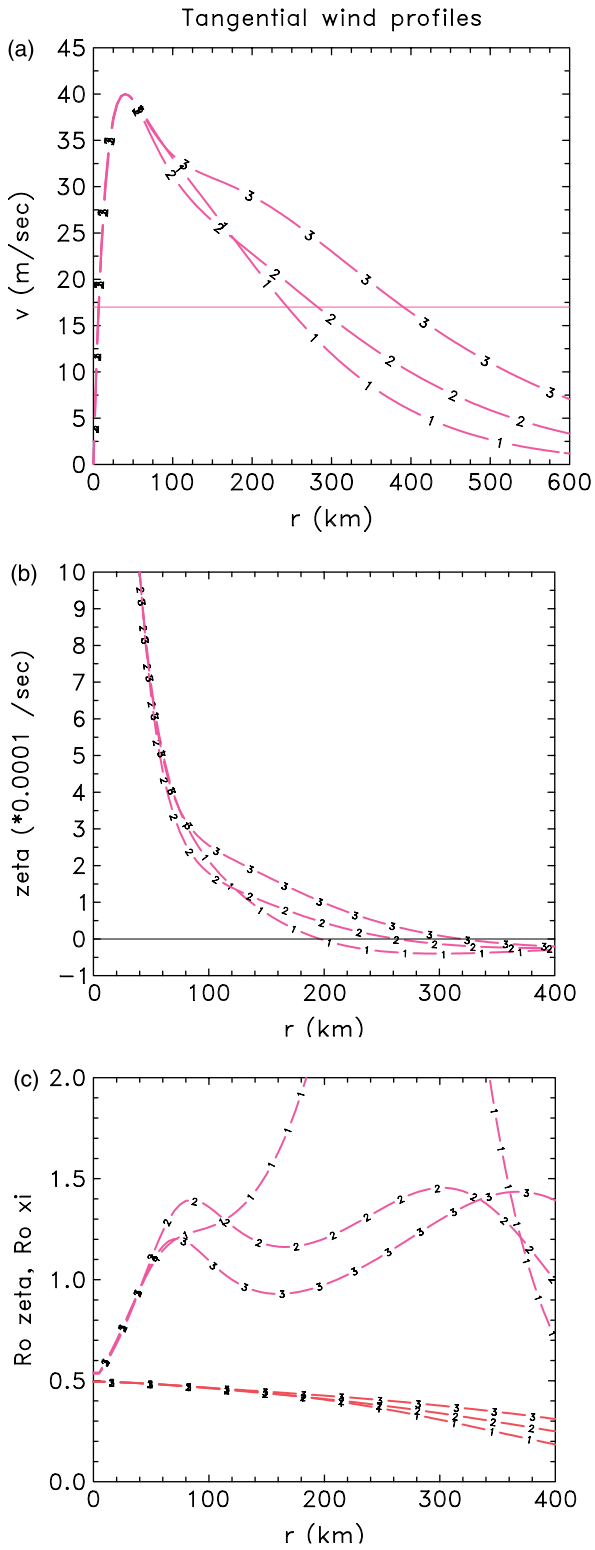

Figure 1. (a) Three tangential wind profiles as a function of radius. The thin horizontal line shows the threshold of gale-force winds. (b) Corresponding profiles of relative vorticity. (c) Radial variation of the Rossby numbers, Ro_Λ (upper three curves) and Ro_Ξ (lower three curves), for these profiles. The maximum of Ro_Λ for profile 1 is 4.5. Numbers on the curves in (b) and (c) refer to the corresponding profile in (a). This figure is available in colour online at www.interscience.wiley.com/journal/qj

estimates for S_u and $S_{v'}$. Figure 1(a) shows a set of tangential wind profiles with the same tangential wind speed maximum of 40 m s^{-1} at the same radius of 40 km, but with varying widths as characterized by the radius of gale force winds, i.e. wind speeds above 17 m s^{-1}. These profiles are detailed in Appendix A. The corresponding radial profiles of the relative vorticity are shown in Figure 1(b) and those of Ro_Ξ and Ro_Λ are shown in Figure 1(c) for the latitude where $f = 5 \times 10^{-1}$. It is clear from the expression for Ro_Ξ that it cannot exceed a magnitude of 0.5 and that it must decrease with radius. On the other hand, Ro_Λ does not have an obvious upper bound and can be quite large if the absolute vorticity at a particular latitude becomes sufficiently small. At least for the profiles shown and for the above value of f, it does not exceed 5.

2.3. The weak friction approximation

We may now envisage a (theoretical) situation where frictional effects are weak in the sense that both S_u and $S_{v'}$ are small compared with unity. Smith and Montgomery (2008) refer to this as the weak friction approximation. In this situation, the nonlinear terms on the left-hand side of Equations (9) and (10) may be neglected provided that Ro_Λ does not appreciably exceed unity (see Table II). In the formal limit where $S_u \ll 1$, $S_{v'} \ll 1$ and $Ro_\Lambda = O(1)$, these two equations reduce to the linear system:

$$-\xi_g v' = K\frac{\partial^2 u}{\partial z^2}, \tag{11}$$

$$\zeta_{ag} u = K\frac{\partial^2 v'}{\partial z^2}. \tag{12}$$

It is of theoretical interest to examine the linear approximation because Equations (11) and (12) are relatively easy to solve analytically (see subsection 2.4 and Appendix B) and because they provide a generalization of the classical Ekman layer theory, the case where $Ro \ll 1$. The corresponding depth-averaged values for u and v in a slab boundary-layer model (Smith, 2003; Smith and Vogl, 2008) indicate that $U \approx V' \approx 0.2V$–$0.3V$, in which case S_u and $S_{v'}$ are not very small compared with unity. Thus, in practice, the solution to the linear equations may not be very accurate. This finding is consistent with that of Smith and Montgomery (2008), who showed that in the case of the slab boundary-layer model the predictions of the linearized equations are poor in relation to solutions of the corresponding nonlinear system.

Unfortunately, the full nonlinear boundary-layer equations (4), (9) and (10) are hard to solve in the steady case because they are parabolic and, unlike the slab case, the radial wind has a different sign at different heights. Nevertheless one can examine the consistency of the linear approximation by estimating the magnitude of the nonlinear terms from the linear solution and comparing these with the corresponding linear terms. As far as we are aware, this has not been done to date and it is the topic of subsection 3.4.

DOI: 10.1002/qj

2.4. Solution of the linear problem

We show in Appendix B that the solution of Equations (11) and (12) has the form

$$u(z) = -\frac{2K}{\zeta_a \delta^2} e^{(-z/\delta)} \{A_2 \cos(z/\delta) - A_1 \sin(z/\delta)\} \quad (13)$$

and

$$v'(z) = e^{(-z/\delta)} \{A_1 \cos(z/\delta) + A_2 \sin(z/\delta)\}, \quad (14)$$

where $\delta = \sqrt{2K/I}$ is a slightly refined scale for the boundary-layer depth, I is the inertial stability parameter, which we defined in the previous subsection in terms of the gradient wind profile, K is an eddy diffusivity, which we assume to be constant with radius and height, and A_1 and A_2 are functions of radius only. These constants are detailed in Appendix B.

3. Some results and an appraisal of the linear theory

In this section we examine aspects of the foregoing analytic solution for one or all of the three gradient wind profiles shown in Figure 1.

3.1. Boundary-layer depth

Figure 2 compares the radial variation of the boundary-layer depth scale, $\delta(r)$, for the three wind profiles and for the parameter values $K = 10$ m^2 s^{-1}, $f = 5 \times 10^{-5}$ s^{-1} and a constant drag coefficient $C_D = 2.0 \times 10^{-3}$. The depths are very similar at large radii and also inside a radius of about 100 km, but they deviate appreciably from one another at intermediate radii, because of the differences in the inertial parameter, which is smaller for narrower vortices on account of the more negative relative vorticity. While the depth for wind profiles 2 and 3 steadily decreases with decreasing radius, that for vortex 1 first increases, before decreasing as the radius decreases further. The initial increase is associated with the fact that the relative vorticity and hence the absolute vorticity and inertial stability for this profile have a minimum at a radius of about 300 km, which implies a local maximum in the boundary-layer depth near this radius. While this maximum is a natural consequence of the scaling, it is not known how realistic it is because of the lack of observational data on the depth of the inflow layer at these radii in a tropical cyclone.

3.2. Vertical velocity above the boundary layer

Figure 3 shows the vertical velocity $w(r)$ evaluated at a height of $z = 2$ km. This quantity can be calculated from the continuity equation, either analytically (see Appendix B) or simply by using finite differences applied to the radial volume flux at radial intervals. The latter method is easier, but we used both methods and verified that they gave the same results. For vortices 2 and 3 the vertical velocity is at a maximum close to, but just outside, the radius of maximum tangential wind speed (at 49 km for vortex 2 and 42 km for vortex 3) with values of 9 cm s^{-1}. Vortex 1 shows also a local maximum of 8.7 cm s^{-1} at 39 km, but the strongest vertical winds are obtained far out from the core region. The profile for w corresponding to vortex 1, the one with a pronounced peak in δ, has a global maximum of 16 cm s^{-1}, twice as large as for the other profiles. However, this maximum occurs at a radius of about 240 km. Significantly, the radius at which the vertical flow changes sign depends markedly on δ, being 280 km for vortex 1, 340 km for vortex 2 and 410 km for vortex 3. The foregoing profiles are similar to those in the slab model for the same tangential wind profile shown in Figures 2(c) and 3(d) of Smith and Montgomery (2008). However the magnitude of the vertical velocity is different because the boundary-layer depth taken for the slab model is not directly equivalent to the one that emerges here. In particular the calculation

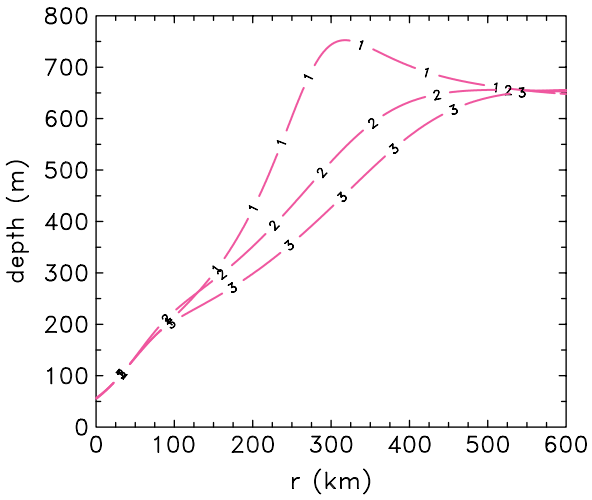

Figure 2. Boundary-layer depth scale δ for the three vortex profiles shown in Figure 1. This figure is available in colour online at www.interscience.wiley.com/journal/qj

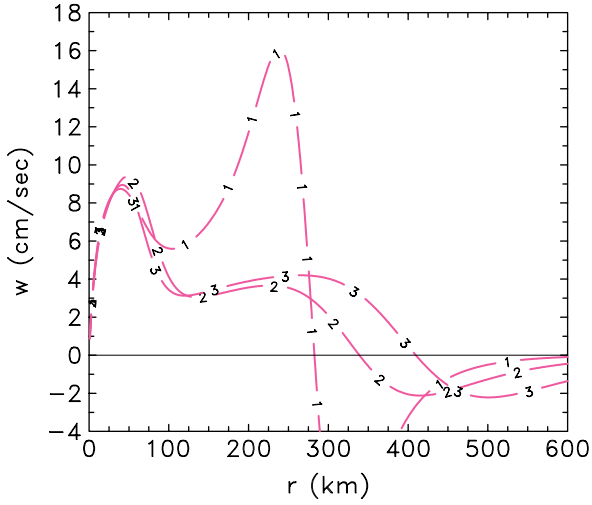

Figure 3. Vertical velocity $w(r)$ for the vortex profiles shown in Figure 1 at $z = 2$ km. This figure is available in colour online at www.interscience.wiley.com/journal/qj

DOI: 10.1002/qj

shown in Figure 2(c) of Smith and Montgomery (2008) assumes a depth that does not vary with radius.

3.3. Boundary-layer structure of vortex 2

We examine now the structure of the boundary layer for vortex 2 in Figure 1 for the values for f, K and C_D defined in subsection 3.1.

Figure 4 shows contour plots of the radial wind speed $u(r, z)$, the tangential wind speed $v(r, z)$, the deviation of the tangential wind from the gradient wind, $v'(r, z) = v(r, z) - v_g(r)$, and the vertical velocity $w(r, z)$ at heights below 2 km, which encompass the boundary layer. The maximum inflow of 13.2 m s^{-1} occurs at a radius of 70 km, about twice the value of r_m, and at a height of about 50 m. The top of the inflow region ($u(r, z) \leq 0$) decreases progressively from about 1.7 km (about 3 scale heights) at a radius of 600 km to less than 150 m inside the radius of maximum tangential wind speed. Above that layer there is weak outflow with maximum wind component ($u(r, z) > 0.5$ m s^{-1}) at radii between 40 km and 100 km and in a height range between 450–850 m.

The tangential winds are slightly larger than the gradient wind in parts of the boundary layer (Figure 4(b)), i.e. they are *supergradient*. The region of supergradient winds is highlighted in Figure 4(c) by the region where $v'(r, z) \geq 0$: this region is seen to extend far out, but the degree by which the winds are supergradient is a maximum in the inner core region ($r < 100$ km) and even there only by a few percent (note that the contour spacing in Figure 4(c) is lower for positive values than for negative values, where the flow is subgradient). The maximum supergradient wind has a value of 1.7 m s^{-1} and occurs at a radius of 55 km at a height of 271 m. The depth of the region of supergradient winds decreases from a height range between about 800–2000 m at radii larger than 400 km to a much shallower height range at smaller radii.

Above the region of supergradient winds the flow becomes slightly subgradient again. This area of subgradient flow coincides approximately with the region of weak outflow ($u(r, z) > 0$) that exists above the inflow layer. Kepert (2001) correctly attributed the occurrence of supergradient winds to the radial transport of absolute angular momentum surfaces by the frictionally induced inflow. Were it not for friction, one would expect the level of maximum supergradient winds to be close to the level at which the radial wind is maximum, assuming that absolute angular momentum surfaces are close to vertical. As seen in Figure 4(a), the maximum radial wind is close to the surface where friction produces the largest deviation of the tangential wind from the gradient wind (Figure 4(c)), and hence the largest net radial force. Since the supergradient winds occur at levels distinct from the maximum inflow it is clear that the vertical diffusion of momentum is required to explain the structure of the

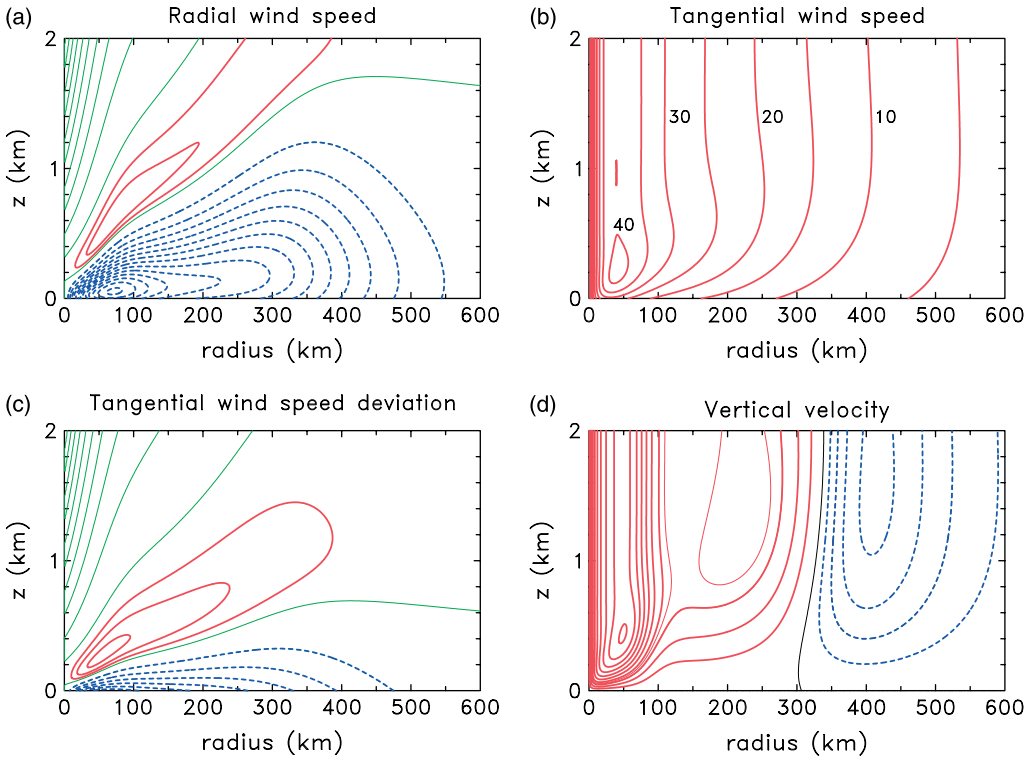

Figure 4. Isopleths of (a) radial and (b) tangential wind components up to a height of 2000 m for vortex profile 2. Contour interval 1 m s^{-1} for negative values of u, 0.2 m s^{-1} for positive values and 5 m s^{-1} for v (selected contour values marked). Dashed curves indicate negative values and solid curves non-negative values. Panel (c) shows the deviation of tangential wind from the gradient wind. Contour interval 2 m s^{-1} for positive values (i.e. supergradient winds) and 0.5 m s^{-1} for negative values (i.e. subgradient winds). Panel (d) shows isopleths of vertical velocity. Contour interval 2 cm s^{-1}. The thin solid curves are the zero contour. The additional thin solid curves in panel (d) have half the contour spacing of the thick lines to highlight the local maximum between 200 and 250 km radius. This figure is available in colour online at www.interscience.wiley.com/journal/qj

DOI: 10.1002/qj

linear boundary layer. For one thing, the absolute angular momentum surfaces are not nearly vertical near the surface and, for another, the absolute angular momentum is not conserved by radial motion in the boundary layer!

Of course, the linear equations for the boundary layer, (11) and (12), express a force balance between the generalized Coriolis force, $(\xi_g v', -\zeta_{ag} u)$, and the vertical diffusion of horizontal momentum, $K(\partial^2/\partial z^2)(u, v)$. At the level of supergradient winds ($v' > 0$), the generalized Coriolis force in the radial momentum equation is radially outwards, i.e. $\xi_g v' > 0$. In the linear boundary layer, this force is balanced by the upward diffusion of negative radial momentum, i.e. $\partial \tau_x / \partial z < 0$, where $\tau_x = K(\partial u/\partial z)$ is the radial stress at height z. A similar force balance exists in the tangential wind direction. In the nonlinear problem, vertical advection will act also to transfer horizontal momentum vertically and Kepert (2001) argues that this is the primary reason for the departure of the linear solution from the nonlinear solution. The calculations described in subsection 3.4 show that radial advection is just as important.

Figure 4(d) shows that there is subsidence into the boundary layer beyond a radius of about 330 km and ascent out of it inside this radius. Furthermore, the radius at which $w(r, z) = 0$ is almost independent of height. The vertical velocity has a local maximum at about 50 km radius, in this case just outside the radius of maximum tangential wind speed of the gradient wind and at a level near the top of the inflow layer. The large radial range of ascent represents a limitation of the linear solution *vis-á-vis* hurricanes as discussed in section 4.

The question arises now: how accurate is the foregoing solution, especially at inner radii where there is strong radial advection? We examine this question below.

3.4. Accuracy of the linear solution

Based on the full solution for $u(r, z)$, $v(r, z)$ and $w(r, z)$, it is possible to assess the accuracy of the linear approximation. Equations (9) and (10) were simplified by omitting the terms

$$t_{n1} = u\frac{\partial u}{\partial r} + w\frac{\partial u}{\partial z} - \frac{v'^2}{r} \tag{15}$$

and

$$t_{n2} = u\frac{\partial v'}{\partial r} + w\frac{\partial v'}{\partial z} + \frac{uv'}{r}, \tag{16}$$

respectively. If we consider $u(r, z)$, $v'(r, z)$ and $w(r, z)$ as approximate solutions of Equations (9) and (10), the terms t_{n1} and t_{n2} can be interpreted as deviation from the exact solution and should be small compared with unity. These expressions can be estimated using the solution of the linearized system. In Figure 5 we compare the magnitude of the terms t_{n1} and t_{n2} with those terms retained:

$$t_{r1} = -\xi_g v'(r, z) \tag{17}$$

and

$$t_{r2} = \zeta_{ag} u(r, z) \tag{18}$$

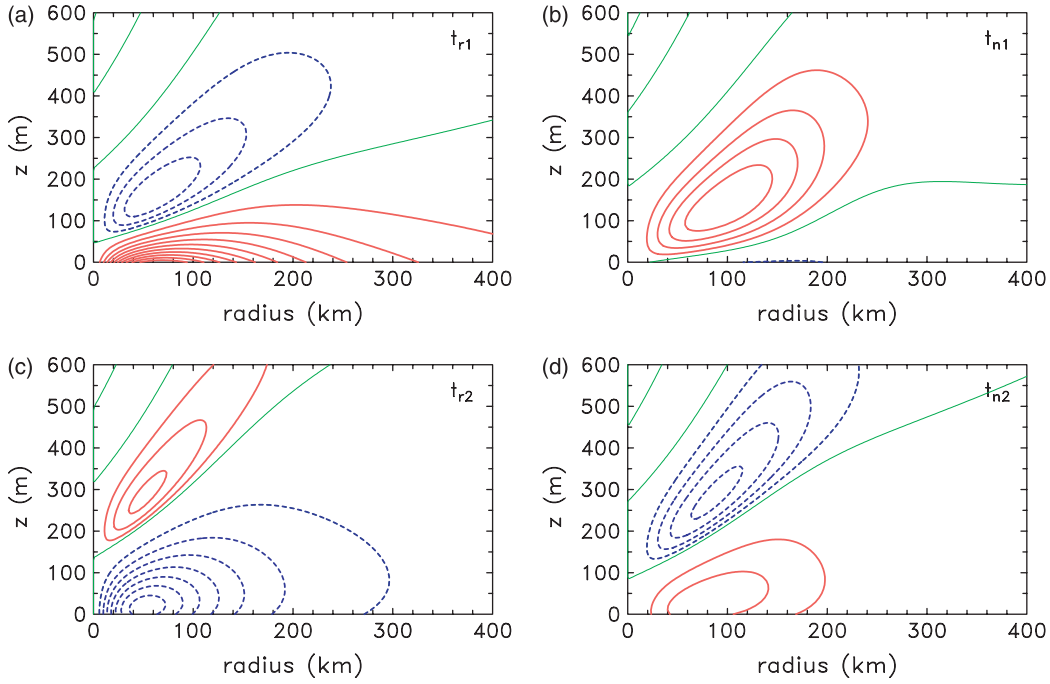

Figure 5. Isopleths of the linear and nonlinear acceleration terms in the radial (upper panels) and tangential (lower panels) momentum equations: (a) t_{r1} (contour interval 2.5×10^{-3} m s^{-2} for positive values (solid/red lines) and 1.0×10^{-3} m s^{-1} for negative values (dashed/blue lines)); (b) t_{n1} (contour interval 1.0×10^{-3} m s^{-2} for positive values, negative values are less than 2.5×10^{-3} m s^{-1}); (c) t_{r2} (contour interval 2.0×10^{-3} m s^{-2} for positive values and 2.0×10^{-4} m s^{-1} for negative values); (d) t_{n2} (contour intervals as in (c)). The thin solid curves are the zero contour. This figure is available in colour online at www.interscience.wiley.com/journal/qj

DOI: 10.1002/qj

respectively. As expected the largest absolute values of t_{r1} and t_{r2} occur in a region close to the surface and at inner radii where the radial and vertical gradients of u and v' are large (Figure 5(a) and (c)). The corresponding isopleths of the neglected terms, t_{n1} and t_{n2}, are shown in Figure 5(b) and 5(d), respectively. It is clear that the neglected terms are comparable in magnitude with those retained over much of the region of interest. (The fact that the zero contours of t_{n1} and t_{n2} do not coincide with those of t_{r1} and t_{r2} makes the comparison in terms of ratios of the neglected to retained terms difficult to interpret.)

The foregoing result is consistent with the scale analysis in section 2.1. From Table II, the relative importance of the neglected terms is characterized by the values of Ro_Ξ and Ro_Λ, which depend on the chosen profile for v_g, together with estimates for S_u and $S_{v'}$. In the weak friction approximation both S_u and $S_{v'}$ are assumed to be small compared with unity. Figure 6 shows the parameters $S_u = |u/v_g|$ and $S_{v'} = |v'/v_g|$ evaluated at the heights at which the radial wind speed and the tangential wind deficit attain their maximum absolute values for the three vortex profiles shown in Figure 1.

The values obtained for S_u and $S_{v'}$ are both largest for vortex 1, with $S_{v'}$ reaching a maximum value of 0.3 and S_u reaching a maximum of 0.83, both at a radius of about 285 km. For vortex 2 and vortex 3, the maxima of S_u and $S_{v'}$ are somewhat smaller and occur at larger radii. In general, the values for S_u are not very small compared with unity and the highest values do not just occur in the core region, but cover much of the radial range shown. This result underpins the findings of the direct comparison of neglected and retained terms shown in Figure 5. Thus the assumptions of the weak friction approximation that $S_u \ll 1$ and $S_{v'} \ll 1$ are not valid for all profiles at all radii. The scale analysis in Table II shows that the nonlinear terms can be neglected if the scales

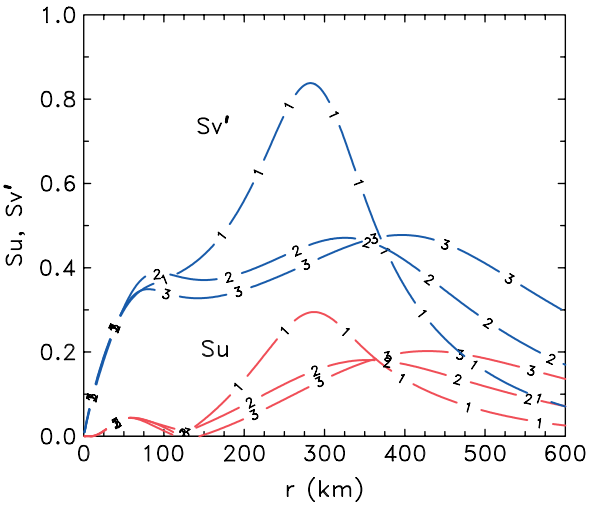

Figure 6. Ratio of the radial to tangential wind speed $S_u = |u/v_g|$ (lower three curves) and ratio of the wind deficit to the gradient wind $S_{v'} = |v'/v_g|$ (upper three curves) evaluated at the height where u and v' reach their maximum absolute values for the three vortex profiles shown in Figure 1. This figure is available in colour online at www.interscience.wiley.com/journal/qj

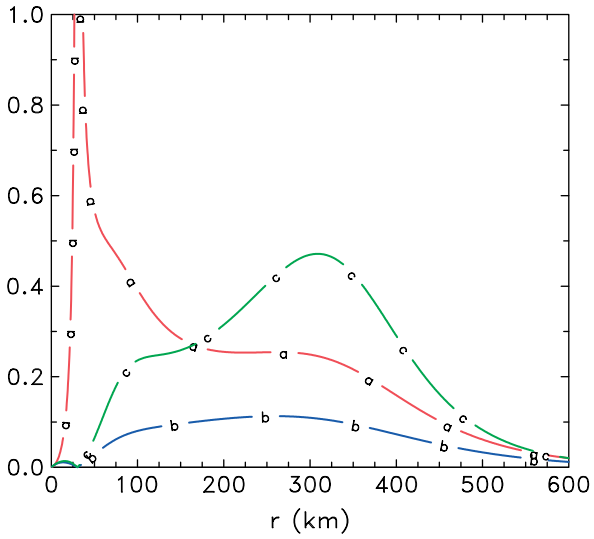

Figure 7. Radial profiles of the scales $S_u^2 S_{v'}^{-1} Ro_\Xi$ (curve a), $S_{v'} Ro_\Xi$ (curve b) and $S_{v'} Ro_\Lambda$ (curve c) for vortex 2. This figure is available in colour online at www.interscience.wiley.com/journal/qj

$S_u^2 S_{v'}^{-1} Ro_\Xi$, $S_{v'} Ro_\Xi$ and $S_{v'} Ro_\Lambda$ are small compared with unity. For vortex 2, this is not the case at most radii, as shown in Figure 7, corroborating the conclusions arrived at above that the linear boundary-layer approximation is inaccurate and does not extend the validity of the classical Ekman layer anywhere near the inner core region of a hurricane.

Kepert (2001, p 2477) stated that '... a limitation of the linear model is the neglect of vertical advection, which is not supported by a scale analysis'. However, the scale analysis presented in Table II suggests that the neglect of radial advection may be an equally important limitation. To examine this feature we calculate the separate contributions of radial and vertical advection to t_{n1} and t_{n2} in the expressions (15) and (16). These contributions are shown in Figure 8 as functions of radius at a height of 100 m, at which level the nonlinear terms are a maximum. It is seen that the maximum values of the vertical advection terms are about twice as large as the maximum values of the radial advection terms, but there are many radii at which the radial advection terms are as large as, or even larger in magnitude than, the vertical advection terms. Evidently the radial advection terms cannot be ignored. The third terms in the expressions for t_{n1} and t_{n2}, i.e. $-v'^2/r$ and uv'/r, respectively, are seen to be smaller than the corresponding advection terms in the inner core region.

4. Discussion

The foregoing analysis points to serious limitations of the linear boundary-layer solution when applied to the inner core of hurricanes, even for radii well beyond the radius of maximum gradient wind speed. However, there is a further limitation that we have *not yet* touched upon. As pointed out by Smith and Vogl (2008), it is probably incorrect to prescribe the tangential wind speed just

DOI: 10.1002/qj

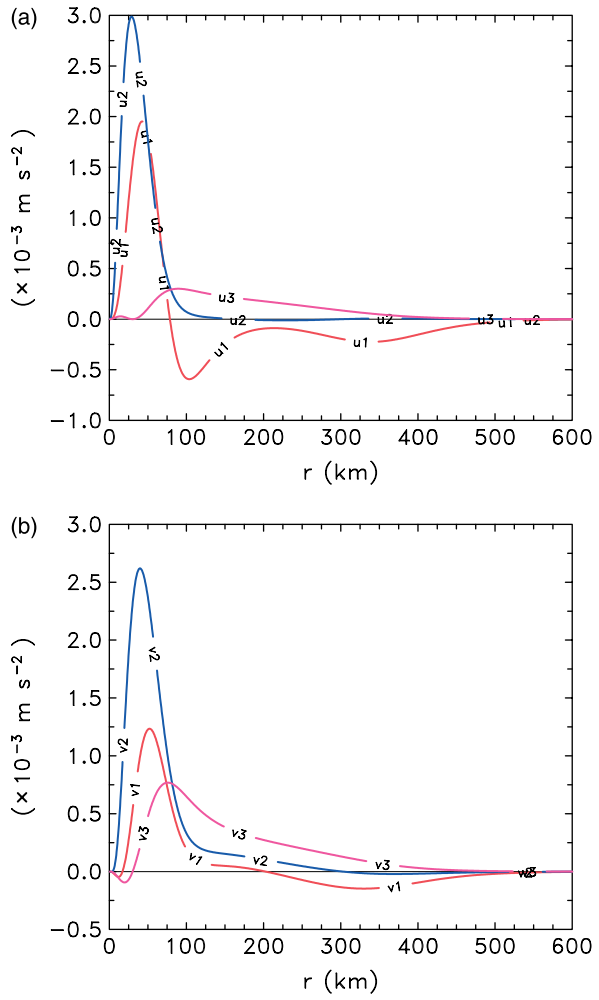

Figure 8. Radial profiles of the radial and vertical advection terms in the expressions for (a) t_{n1} and (b) t_{n2}. In (a), u1 refers to $u(\partial u/\partial r)$ and u2 to $w(\partial u/\partial z)$, while in (b) v1 refers to $u(\partial v'/\partial r)$ and v2 to $w(\partial v'/\partial z)$. Shown also for comparison are the additional terms in the expressions, i.e. $-v'^2/r$ in t_{n1} and uv'/r in t_{n2}, which are labelled u3 and v3, respectively. This figure is available in colour online at www.interscience.wiley.com/journal/qj

above the boundary layer in the inner region, where the flow exits the boundary layer. Many previous boundary-layer models have taken this approach (e.g. Smith, 1968; Ooyama, 1969; Leslie and Smith, 1970; Bode and Smith, 1975; Shapiro, 1983; Kepert, 2001; Smith, 2003), but the consequences thereof have not been investigated or discussed in detail. Presumably, with this limitation in mind, Kepert and Wang (2001) used a boundary condition that constrains the vertical gradient of the radial and tangential velocity components to be zero at the top of their computational domain. Nevertheless, because the radial motion at this boundary turns out to be close to zero (see their Figure 2), the tangential wind speed must be close to the gradient wind at this boundary.

We concur with Kepert and Wang (2001) that it is more reasonable to suppose that boundary-layer air carries its momentum with it as it ascends out of the boundary layer because this boundary is an 'outflow boundary' of the problem. Unfortunately, it is not possible to accommodate a zero vertical-gradient constraint in the analytic solution of the linear model. Since the radius at which the vertical motion reverses sign at the top of the boundary layer occurs relatively far from the vortex centre in the linear model, the inability to apply a zero vertical-gradient constraint further limits the usefulness of the model when applied to hurricanes. These remarks apply presumably to the extension of the linear model to non-axisymmetric flow worked out by Kepert (2001).

As argued by Smith and Vogl (2008), the same limitation does not exist in a slab boundary-layer model because the boundary-layer wind and gradient wind are not the same at the top of the boundary layer, even though the radial pressure gradient in the boundary layer is the same as that above (see Smith and Montgomery (2008) for a scale analysis for the slab boundary layer). Nevertheless there are still challenging issues involved in properly coupling a slab boundary layer to the flow above (Smith *et al.* 2008).

Throughout this article we have assumed the turbulent diffusivity to be constant with height and radius, a feature that is a gross simplification. We believe that the assumption that the diffusivity is constant with height is adequate for present purposes when combined with a bulk drag formulation of the surface layer (see e.g. Leslie and Smith, 1970; Bode and Smith, 1975). Keeping K constant with radius is potentially more serious as one would certainly expect turbulence levels to rise as the wind speeds increase significantly with decreasing radius. Unfortunately observations provide little guidance on the magnitude of this increase. In view of the result that the linear boundary-layer theory breaks down in the region of strong winds, it is questionable whether one would learn much more from calculations in which such an increase in K is postulated. Nevertheless, the scaling analysis in section 2.1 suggests that any increase will be reflected in a commensurate increase in the boundary-layer depth above that predicted assuming a radially constant K. Similar remarks apply to the representation of the surface drag coefficient. Here we have used a constant value, whereas observations suggest that it increases linearly with near-surface wind speed, at least up to wind speeds of about 20 m s^{-1}, after which it remains approximately constant (see Black *et al.* 2006). However the behaviour of C_D has been determined only for wind speeds up to about 30 m s^{-1}. We could have used the latest estimates for the variation of C_D in the foregoing calculations, but the additional degree of sophistication seems unwarranted in view of the limitations of the linear theory that we have demonstrated.

5. Conclusions

We have derived the boundary-layer equations for a hurricane from the Navier–Stokes equations, assuming that the turbulent transfer of momentum can be characterized by a constant eddy diffusivity in conjunction with a bulk representation of surface drag. The derivation is based on a detailed scale analysis of the Navier–Stokes equations.

DOI: 10.1002/qj

We showed how a linear form of the boundary-layer equations that has been studied by several previous authors can be obtained as a weak friction limit of the full equations. The weak friction limit formally assumes that the radial and perturbation tangential velocity components are small compared with the gradient wind speed above the boundary layer and that the local Rossby number based on the absolute vorticity of the gradient wind is of order unity or less.

We showed height–radius plots of the three velocity components derived from an analytic solution of the linear boundary-layer equations. Interesting features are the presence of supergradient winds at all radii and a vertical velocity that has a weak local maximum just at the top of the inflow layer near the radius of maximum gradient wind speed. The radial profile of vertical velocity at the top of the boundary layer for three tangential wind profiles is similar in shape to those in a slab version of the linear model. However, a recent study of the slab model has shown that the profiles of vertical velocity in the linear model are unrealistic compared with that in the nonlinear version. In particular, the radius at which the subsidence changes to ascent in the linear solution is far too large. This would have important ramifications for the integrity of the linear solution in the continuous model, because the upper boundary condition that the tangential wind tends to the gradient wind and the radial wind tends to zero at the top of the boundary layer cannot be justified when there is ascent out of the boundary layer.

We showed that the linear solution is not self-consistent over a considerable range of radii because the magnitude of the nonlinear terms calculated from this solution is not much smaller than the linear terms themselves. This conclusion is supported also by considering the relative magnitude of terms in the scale analysis. These remarks apply presumably also to non-axisymmetric extensions of the linear theory.

Acknowledgements

We thank Michael Montgomery for his insightful comments on the first draft of the manuscript. Part of this work was carried out during a visit by the authors to the NOAA/AOML Hurricane Research Division in Miami. Our thanks go to the Director, Frank Marks, and colleagues for providing us with a stimulating working environment. We also thank the two anonymous reviewers for their careful reading of the original manuscript and their constructive comments on it. The first author gratefully acknowledges a doctoral stipend provided by the Munich Reinsurance Company.

Appendix A: Tangential wind profiles, $v_g(\mathbf{r})$

In the calculations described above we examined a set of three profiles for the gradient wind of the form

$$v_g(r) = V_1 s e^{-\alpha_1 s} + V_2 s e^{-\alpha_2 s}, \quad \text{where} \quad s = \frac{r}{r_m},$$

where V_1, V_2, α_1 and α_2 are constants, chosen so that the maximum wind speed v_m is the same (40 m s^{-1}) for each profile and occurs at a radius $r_m = 40$ km. In terms of the parameters $\mu = V_2/v_m$ and α_2 we can calculate α_1 and V_1 using

$$\left.\begin{aligned} \alpha_1 &= (1 - \mu\alpha_2 e^{-\alpha_2})/(1 - \mu e^{-\alpha_2}), \\ V_1 &= v_m e^{\alpha_1}(1 - \mu e^{\alpha_2}). \end{aligned}\right\} \tag{A1}$$

The three wind profiles shown in Figure 1 are specified by the values for (μ, α): (0.8, 0.4), (0.5, 0.3), and (0.5, 0.25). These profiles are all inertially stable ($\xi_g \zeta_{ag} > 0$) for the Coriolis parameter used ($f = 5.0 \times 10^{-5}$ s^{-1}).

Appendix B: Solution of the linear model

Equations (9) and (10) may be readily solved by eliminating either u or v' to give a fourth-order ordinary differential equation for the other variable. For example, eliminating u gives an equation for v':

$$\frac{\partial^4 v'}{\partial z^4} + \frac{I^2}{K^2} v' = 0, \tag{B1}$$

and then u is given by

$$u(z) = \frac{K}{\zeta_{ag}} \frac{\partial^2 v'(z)}{\partial z}. \tag{B2}$$

Kepert (2001) showed that the solution of Equation (B1) that is bounded as $z \to \infty$ has the form

$$v'(z) = V_1 e^{-(1-i)z/\delta} + V_2 e^{-(1+i)z/\delta}, \tag{B3}$$

where V_1 and V_2 are complex constants. This may be written in the form

$$v'(z) = e^{-z/\delta}[A_1 \cos(z/\delta) + A_2 \sin(z/\delta)], \tag{B4}$$

where A_1 and A_2 are constants determined by a second boundary condition, e.g. for $z = 0$. The corresponding solution for u is obtained by substituting (B4) into (B2), i.e.

$$u(z) = -\frac{2K}{\zeta_{ag}\delta^2} e^{(-z/\delta)}[A_2 \cos(z/\delta) - A_1 \sin(z/\delta)]. \tag{B5}$$

We apply a slip boundary condition at the surface ($z = 0$) with a quadratic drag law for the surface stress. Defining $\mathbf{u} = (v_g + v', u)$ and a drag coefficient C_D, this condition takes the form

$$K \frac{\partial \mathbf{u}}{\partial z} = C_D |\mathbf{u}|_{z=0} \mathbf{u} \qquad \text{at} \quad z = 0. \tag{B6}$$

Substituting the expressions (B5) for u and (B4) for v', we obtain

$$\frac{\partial v'}{\partial z}|_{z=0} = \frac{(A_2 - A_1)}{\delta} \quad \text{and} \quad \frac{\partial u}{\partial z}|_{z=0} = \frac{2K}{\zeta_{ag}\delta^2} \frac{(A_1 + A_2)}{\delta}.$$

DOI: 10.1002/qj

With

$$|\mathbf{u}|_{z=0} = \sqrt{(v_g + A_1)^2 + \left(\frac{2K}{\zeta_{ag}\delta^2}\right)^2 A_2^2},$$

the boundary condition at the surface gives two algebraic equations:

$$\left.\begin{aligned} A_2 - A_1 &= \nu\sqrt{(\ldots)}(v_g + A_1), \\ A_2 + A_1 &= -\nu\sqrt{(\ldots)}A_2, \end{aligned}\right\} \tag{B7}$$

where

$$\sqrt{\cdots} = \sqrt{\left(1 + \frac{A_1}{v_g}\right)^2 + \left(\frac{2K}{\zeta_{ag}\delta^2}\right)^2 \left(\frac{A_2}{v_g}\right)^2}$$

and $\nu = C_D R_e$ with $R_e = v_g\delta/K$. These two equations may be solved to calculate the coefficients A_1 and A_2 and to obtain the full solutions $(u(r, z), v(r, z), w(r, z))$ in terms of the local tangential wind speed at the top of the boundary layer, $v_g(r)$. The vertical velocity $w(r, z)$ is obtained by integrating the continuity equation (4) with respect to height to give

$$w(r, z) = -\frac{\partial}{\partial r}\left(\frac{1}{r}\int_0^z ru\,\mathrm{d}z\right),$$

where, using (B5),

$$\int_0^z ru\,\mathrm{d}z = \frac{\mathrm{e}^{-z/\delta}K}{\delta\zeta_{ag}} \times [(A_1 - A_2)\cos(z/\delta) + (A_1 + A_2)\sin(z/\delta)]. \tag{B8}$$

References

Black PG, D'Asaro EA, Drennan WM, French JR. Niiler PP, Sanford TB, Terrill EJ, Walsh EJ, Zhang JA. 2006. Air–sea exchange in hurricanes: synthesis of observations from the coupled boundary layer air–sea transfer experiment. *Bull. Am. Meteorol. Soc.* **88**: 357–374.

Bode L, Smith RK. 1975. A parameterization of the boundary layer of a tropical cyclone. *Boundary-Layer Meteorol.* **8**: 3–19.

Carrier GF. 1971. Swirling flow boundary layers. *J. Fluid Mech.* **49**: 133–144.

Eliassen A. 1971. On the Ekman Layer in a circular vortex. *J. Meteorol. Soc. Jpn* **49**: 784–789.

Eliassen A, Lystadt M. 1977. The Ekman layer of a circular vortex: a numerical and theoretical study. *Geophysica Norvegica* **31**: 1–16.

Emanuel KA. 1997. Some aspects of hurricane inner-core dynamics and energetics. *J. Atmos. Sci.* **54**: 1014–1026.

Kepert JD, Wang Y. 2001. The dynamics of boundary layer jets within the tropical cyclone core. Part II: nonlinear enhancement. *J. Atmos. Sci.* **58**: 2485–2501.

Leslie LM, Smith RK. 1970. The surface boundary layer of a hurricane – Part II. *Tellus* **22**: 288–297.

Miller BI. 1965. A simple model of the hurricane inflow layer. *Weather Bureau Technical Note 18-NHRL 75*. US Dept of Commerce, National Hurricane Research Laboratory: Miami, Florida.

Montgomery MT, Snell HD, Yang Z. 2001. Axisymmetric spindown dynamics of hurricane-like vortices. *J. Atmos. Sci.* **58**: 421–435.

Ooyama KV. 1969. Numerical simulatoion of the life-cycle of tropical cyclones. *J. Atmos. Sci.* **26**: 3–40.

Rosenthal SL. 1962. A theoretical analysis of the field motion in the hurricane boundary layer. *National Hurricane Research Project Report No 56*. US Dept of Commerce, National Hurricane Research Laboratory: Miami, Florida.

Shapiro LJ. 1983. The asymmetric boundary layer under a translating hurricane. *J. Atmos. Sci.* **40**: 1984–1998.

Smith RK. 1968. The surface boundary layer of a hurricane. *Tellus* **20**: 473–483.

Smith RK. 2003. A simple model of the hurricane boundary layer. *Q. J. R. Meteorol. Soc.* **129**: 1007–1027.

Smith RK, Montgomery MT. 2008. Balanced boundary layers used in hurricane models. *Q. J. R. Meteorol. Soc.* **134**: 1385–1395.

Smith RK, Vogl S. 2008. A simple model of the hurricane boundary layer revisited. *Q. J. R. Meteorol. Soc.* **134**: 337–351.

Smith RK, Montgomery MT, Vogl S. 2008. A critique of Emanuel's hurricane model and potential intensity theory. *Q. J. R. Meteorol. Soc.* **134**: 551–561.

Smith RK, Montgomery MT, Nguyen SV. 2009. Tropical cyclone spin up revisited. *Q. J. R. Meteorol. Soc.* **135**: in press. DOI: 10.1002/qj.428.